Water Air Soil Pollut (2020) 231: 103
https://doi.org/10.1007/s11270-020-04473-6

Adsorption Behavior and Mechanism of Oxytetracycline on Rice Husk Ash: Kinetics, Equilibrium, and Thermodynamics of the Process

Christhell A. Andrade · Luis Angel Zambrano-Intriago · Nelson S. Oliveira · Judite S. Vieira · Luis Santiago Quiroz-Fernández · Joan Manuel Rodríguez-Díaz

Received: 18 September 2019 / Accepted: 13 February 2020 / Published online: 2 March 2020

Abstract The main objective of the present study is to determine the kinetics, thermodynamics, and adsorption mechanism of the oxytetracycline (OTC) on rice husk ash (RHA). The adsorbent was characterized by scanning electronic microscopy, Fourier transform infrared spectroscopy, and nitrogen physisorption. Batch studies were carried out to evaluate the influence of the adsorbent dose, initial concentration, contact time, temperature, and initial pH. RHA was characterized as having heterogeneous, fibrous, and porous particles, consisting predominantly of silica. The removal of OTC depends on the pH of the medium, which is favored at acid pH values. The kinetic data followed the Bangham model, which indicated an OTC diffusion in the pores of RHA, although this was not the only process, as demonstrated through the use of the Weber-Morris model (IPD model). The Sips isotherm best represents the experimental results of the equilibrium study. It was found that the adsorption process was spontaneous and endothermic. The highest adsorption capacity was found at a pH in the range of 4–6, when the OTC is in its zwitterion form and the surface of the RHA is positively charged, thus permitting electrostatic interactions and the formation of hydrogen

Electronic supplementary material The online version of this article (https://doi.org/10.1007/s11270-020-04473-6) contains supplementary material, which is available to authorized users.

C. A. Andrade · L. A. Zambrano-Intriago · J. M. Rodríguez-Díaz
Laboratorio de Análisis Químicos y Biotecnológicos, Instituto de Investigación, Universidad Técnica de Manabí, Portoviejo, Ecuador

L. A. Zambrano-Intriago
e-mail: luiszamint@gmail.com

C. A. Andrade · N. S. Oliveira · J. S. Vieira
Laboratory of Separation and Reaction Engineering-Laboratory of Catalysis and Materials (LSRE-LCM), School of Technology and Management (ESTG), Polytechnic Institute of Leiria, 2411-901 Leiria, Portugal

N. S. Oliveira
e-mail: nelson.oliveira@ipleiria.pt

J. S. Vieira
e-mail: judite.vieira@ipleiria.pt

C. A. Andrade (✉)
Facultad de Ciencias Zootécnicas, Universidad Técnica de Manabí, Portoviejo, Ecuadore-mail: chris.andraded@gmail.com

L. S. Quiroz-Fernández
Instituto de Postgrado, Universidad Técnica de Manabí, Portoviejo, Ecuadore-mail: santyqf@gmail.com

J. M. Rodríguez-Díaz
Departamento de Procesos Químicos, Facultad de Ciencias Matemáticas, Físicas y Químicas, Universidad Técnica de Manabí, Portoviejo, Ecuador
J. M. Rodríguez-Díaz (✉)

Programa de Pós-graduação em Engenharia Química, Universidade Federal da Paraíba, João Pessoa 58051-900, Brazile-mail: joanrd9@yahoo.com

bonds between the adsorbent and adsorbate molecules. These findings demonstrate the potential of rice husk ash to remove oxytetracycline from water.

Keywords Oxytetracycline · Rice husk ash · Electrostatic interactions · Hydrogen bonds

1 Introduction

As the pharmaceutical industry has developed, various types of drugs, and particularly antibiotics, have been detected in bodies of water (Zhang et al. 2016). This type of pollutant is considered to be an emerging pollutant and has, therefore, received a considerable amount of attention regarding its removal. Antibiotics are widely used in human and veterinary medicine, but also as a feed supplement to promote growth in livestock and the aquaculture industry. Tetracyclines, and especially oxytetracycline (OTC), have been reported to be the antibiotics most frequently used worldwide owing to their broad spectrum antimicrobial activity (Ratasuk et al. 2012). However, 50–80% (Kong et al. 2012; Cheng et al. 2013) of OTC cannot be adsorbed and is discharged unmetabolized via feces and urine. Oxytetracycline is difficult to remove from water owing to its high solubility, the naphthol ring main structure, its ability to form complexes with other species, and its ionic state pH dependence (Leal 2017; Ahmed 2017). The presence of OTC in surface water affects its self-depuration because the nitrification process is inhibited (Halling-Sørensen et al. 2002). Moreover, the continuous input of OTC into water creates antibiotic resistance and may be toxic for animals and humans, causing allergies and intoxications (Ahmed 2017; Cheng et al. 2013). Although the amount of antibiotics in the environment is relatively low, its persistence constitutes a potential risk.

Various methods have been used to remove OTC, including ozonation, electrochemical processes, membrane technologies, and advanced oxidation processes (Malakootian et al. 2016). Although these methods can be efficient, they usually involve high costs and can produce intermediate products that are even more toxic than the original compound (Ahmed et al. 2015; Li et al. 2015). Adsorption has arose as an attractive option for the removal of emerging pollutants because it has high removal efficiency, low initial costs, simplicity of design, is easy to operate, and is not selective to toxic substances (Malakootian et al. 2016). The most widely used adsorbent is activated carbon owing to its high efficiency as regards the removal of organic compounds (Villar da Gama et al. 2018). However, it is limited by its high production and regeneration costs and the loss of efficiency after the regeneration process (Acevedo et al. 2015; Aljeboree et al. 2017). Several low cost and easily accessible materials, which are principally agricultural biomasses, are, therefore, currently being studied for the removal of OTC at different operating conditions, and a good performance has been reported for materials with or without previous treatment.

Recent studies have reported strong interactions between OTC and various materials such as kaolinite (Song et al. 2019), willow residues (Wang et al. 2018), microalgae (Santaeufemia et al. 2016), or aerobic granular sludge (Mihciokur and Oguz 2016), but until now no work has studied the use of rice biomass for OTC adsorption.

Rice covers about 1% of the Earth's surface, is the third biggest crop worldwide (Foo and Hameed 2009), and is one of the primary staple foods. It is one of the most important products in Ecuador, occupying approximately 15.34% of the cultivated area (Monteros et al. 2014). Around 20% of the net weight of rice corresponds to its husk, whose disposal constitutes an environmental problem. Rice husk is a residue whose degradation is slow. It is composed of cellulose, hemicelluloses, lignin, and mineral ash (20%) with a high silica content (96.34%) in the ashes (Ahmaruzzaman and Gupta 2011), signifying that in addition to other uses as fuel and construction materials, the rice biomass and its ashes could be good low-cost biosorbents. The objective of this study is, therefore, to evaluate the best experimental conditions, kinetics, equilibrium, thermodynamics, and adsorption mechanism for OTC in rice husk ash (RHA).

2 Materials and Methods

2.1 Materials and Quantification Methodology

The oxytetracycline (OTC) hydrochloride used for the experiments was of an analytical grade and was obtained from Sigma-Aldrich (USA). Solvents, including methanol, acetonitrile, and formic acid, were of an HPLC grade (Merck). The NaOH and HCl used were of an analytical grade (Merck). The ultrapure water used for solution preparation and glassware cleaning was obtained using Thermo Scientific Barnstead EasyPure II equipment.

The quantification of OTC in solution was carried out by means of high-performance liquid chromatography (HPLC), using a Thermo Accela chromatograph equipped with an automatic injector, a quaternary pump, and a UV-VIS photodiode array detector (PDA). The analyses were performed with a C18 column, model 25,005–104,630 from Thermo Fisher (5 μm, 100 mm × 4.6 mm), with an injection volume of 10 μL, at 25 °C. A binary mobile phase composed of acetonitrile and acidified water (pH 2, Formic Acid) (80:20, *v*:*v*) was used at a constant flow rate of 0.900 mL.min^{-1} with a retention time of 2.18 min. The detection was operated at 350 nm.

2.2 Adsorbent Characterization

The rice husk ash (RHA) used as adsorbent in this study was obtained from the "Charapotó" rice mill in Manabí, Ecuador, and was collected at particular time intervals throughout the rice season. The raw RHA was sieved and used without prior treatment. The particle size of the RHA was determined by means of granulometry using a sieve column (Humboldt Standard) with standard sieve sizes (N°) of 12, 16, 20, 30, 40, 50, 100, and 200. The morphological characteristics of the RHA were determined through the use of scanning electron microscopy coupled with energy-dispersive X-ray spectroscopy SEM/EDX (Quanta 400FEG ESEM/EDAX Genesis X4M). The samples were coated with Au/Pd for 100 s and with a 15 mA current. The surface functional groups before and after adsorption were identified by employing the attenuated total reflectance (ATR) technique, in the wavelength range from 4000 to 400 cm^{-1}, using a Thermo Nicolet FT-IR. The specific surface area was calculated from the N_2 adsorption/desorption isotherms by using a surface area analyzer (Nova Station Quantachrome) and applying the Brunauer-Emmett-Teller (BET) equation (Rodríguez-Díaz et al. 2015). The surface of the RHA was characterized by the point of zero charge (pH_{pzc}), which is the pH at which the sorbent surface charge has a zero value. The pH_{pzc} was determined by means of the powder addition method (Cristiano et al. 2011), which consisted of shaking 0.10 g of RHA in contact with modified pH distilled water at 300 rpm. The pH was adjusted by adding NaOH (0.1 M) or HCl (0.1 M) and was measured using a Fisher Scientific Accumet-AB150 pHmeter.

2.3 Adsorption Tests

The effects of time, adsorbent dose, pH of the initial solution, initial concentration, and temperature were assessed in batch adsorption experiments. All the experiments were carried out by shaking 100 mL of OTC solution of the required concentration with a dose of RHA in a 250 mL Erlenmeyer flask wrapped up in aluminum foil to prevent photodegradation, using an orbital shaker (Thomas Scientific) at a speed of 300 rpm. The shaking speed of 300 rpm was decided based on preliminary tests and published literature (Jaerger et al. 2015; Álvarez-Torrellas et al. 2016; Bhowmick et al. 2015)

The adsorbent dose effect was studied by agitating a 50 mg L^{-1} OTC solution with different doses of RHA, ranging from 0.20 to 3.0 g in an interval of 0.20 g, for 360 min, at 298 K and natural pH of the initial solution (4.24). The effect of the pH on the rate of OTC removal was analyzed in the pH range of 2–10. The initial solution pH was adjusted by adding HCl (0.1 M) or NaOH (0.1 M) solutions. The experiments were performed by shaking 1.6 g of RHA, selected based in the adsorbent dosage study, with 100 mL OTC solution with a modified pH, at three different concentrations (50, 100, and 200 mg L^{-1}), for 360 min at 298 K. The initial concentrations tested for OTC were from 20 to 160 mg L^{-1}, for various times of between 3 and 540 min, at 298 K and with the natural pH of the solution. The effect of temperature for the OTC adsorption onto the RHA was studied for 298, 318, and 328 K, by mixing 1.6 g of RHA with 100 mL of OTC solution at different initial concentrations (20–160 mgL^{-1}) and shaking until equilibrium time.

After the predetermined contact time (effects of time), the flasks were removed from the shaker, and the supernatant was filtered through 0.45 μm of polyvinylidene fluoride (PVDF) syringe filter and analyzed by means of HPLC. All the experiments were carried out as triplicated assays to ensure the reliability of the results. The amounts of OTC adsorbed onto the RHA were calculated by employing the Eq. (1) and Eq. (2)

$$q = \frac{(C_o - C_t)}{w} V \tag{1}$$

$$\%R = \frac{(C_o - C_t)}{C_o} \times 100 \tag{2}$$

where q (mg g^{-1}) is the adsorption capacity of the system adsorbate-adsorbent, C_o (mg L^{-1}) is the initial adsorbate concentration, C_t (mg L^{-1}) is the adsorbate concentration at time t (min), V (mL) is the volume of solution, and w (mg) is the mass of adsorbent. R is the percentage of removal.

2.4 Adsorption Kinetics and Equilibrium

The adsorption kinetics and equilibrium experiments were carried out separately, applying the best conditions determined by the adsorption tests for the OTC (100 mL of solution; concentration from 20 to 160 mg L^{-1}; 1.6 g of adsorbent). The experimental data obtained were adjusted to non-linear models of adsorption kinetics and equilibrium using the Statistica 10.0 software. Adsorption kinetic and equilibrium models are presented in Supporting Information (SI) ***S1***.

2.5 Adsorption Thermodynamics

The thermodynamic parameters, change of enthalpy ($\Delta H°$), change of entropy ($\Delta S°$), and Gibbs free energy ($\Delta G°$), were calculated following the equations presented in SI ***S2***.

3 Results and Discussion

3.1 RHA Characterization

The granulometric analysis enabled us to discover that approximately 53% of the RHA consists of particles from 0.150 to 0.430 mm (Fig. S1). In order to ensure the homogeneity of the particle size and a larger mass transfer area, only the particles comprised between these fractions (0.150 and 0.430 mm) were selected for the development of all subsequent tests. The surface charge of the adsorbent material is related to the pH_{pzc} and the pH of the contact solution. The pH_{pzc} value found following the powder addition method (Cristiano et al. 2011) was 8. If the pH of the medium is lower than the point of zero charge ($pH < pH_{pzc}$), the surface of the solid will have a predominance of positive charges, thus favoring interactions with the anions present in the medium. However, if the pH of the medium is greater than the point of zero charge of the solid ($pH > pH_{pzc}$), there will be a predominance of negative charges on the surface, which will favor interactions with cations. The microstructure of the RHA is shown in Fig. 1 a. The particles have a rectangular structure, curved inwards, with well-arranged corrugated and spiky cuticles on the external surface. The internal surface of the particles has an irregular fibrous and porous structure, in which the spaces between the fibers and the pores are large and heterogeneous. The presence of meso- and macropores is favorable to the adsorption of large organic molecules, such as oxytetracycline. Similar characteristics have been reported for the rice husk ash used in other works published in scientific literature (Ahmaruzzaman and Gupta 2011; Hadipramana et al. 2016). The EDX spectrum (Fig. 1b**)** shows that the main components of RHA are silica and oxygen, which are concentrated in the form of SiO_2 in the domed protuberances of RHA (Park et al. 2003), and carbon, potassium, and chloride were also found in lower concentrations in the RHA.

The BET adsorption/desorption isotherms obtained by means of nitrogen physisorption (Fig. 1c) confirm the presence of mesopores, which are, according to the Brunauer et al. (1940), they are classified as type IV, typical of mesoporous materials. The low surface area determined, with a value of 33.796 m^2 g^{-1}, is owing to the low concentration of carbon present in RHA (Fig. 1b**).**

The infrared spectra of the RHA before and after OTC adsorption are shown in Fig. 1 d. Before the adsorption, the most prominent peaks correspond to the Si-O-Si, Si-H, and Si-O groups. The peak of greater intensity is observed in the 1051.26 cm^{-1} band, corresponding to the stretching vibrations of the siloxane group (Si-O-Si), and the peak observed at 793.56 cm^{-1} corresponds to the presence of Si-H from the silane group. A peak corresponding to Si-O is observed at 557.87 cm^{-1} and is attributed to the high content of SiO_2 present in the ashes. The presence of silicon groups on the surface of the RHA corresponds with those reported in literature, which states that 95% of the composition of the rice husk ash is silicon (Ahmaruzzaman and Gupta 2011) and is also evidenced by the EDX spectrum (Fig. 1b), which shows that SiO_2 is the main component of RHA. After the adsorption process, these peaks shift and stretch their intensity, and new peaks corresponding to the groups -Si-OH, -OH, -CO- and -C-H appear. The displacement of an increase in the peak at 3360.69 cm^{-1} can be attributed to the stretching of the OH bond of the silanol group (Si-OH) and the water adsorbed on the surface of the RHA. The peak at 2360.56 cm^{-1} disappears after adsorption with a peak appearing at 1875.07 cm^{-1} associated with the

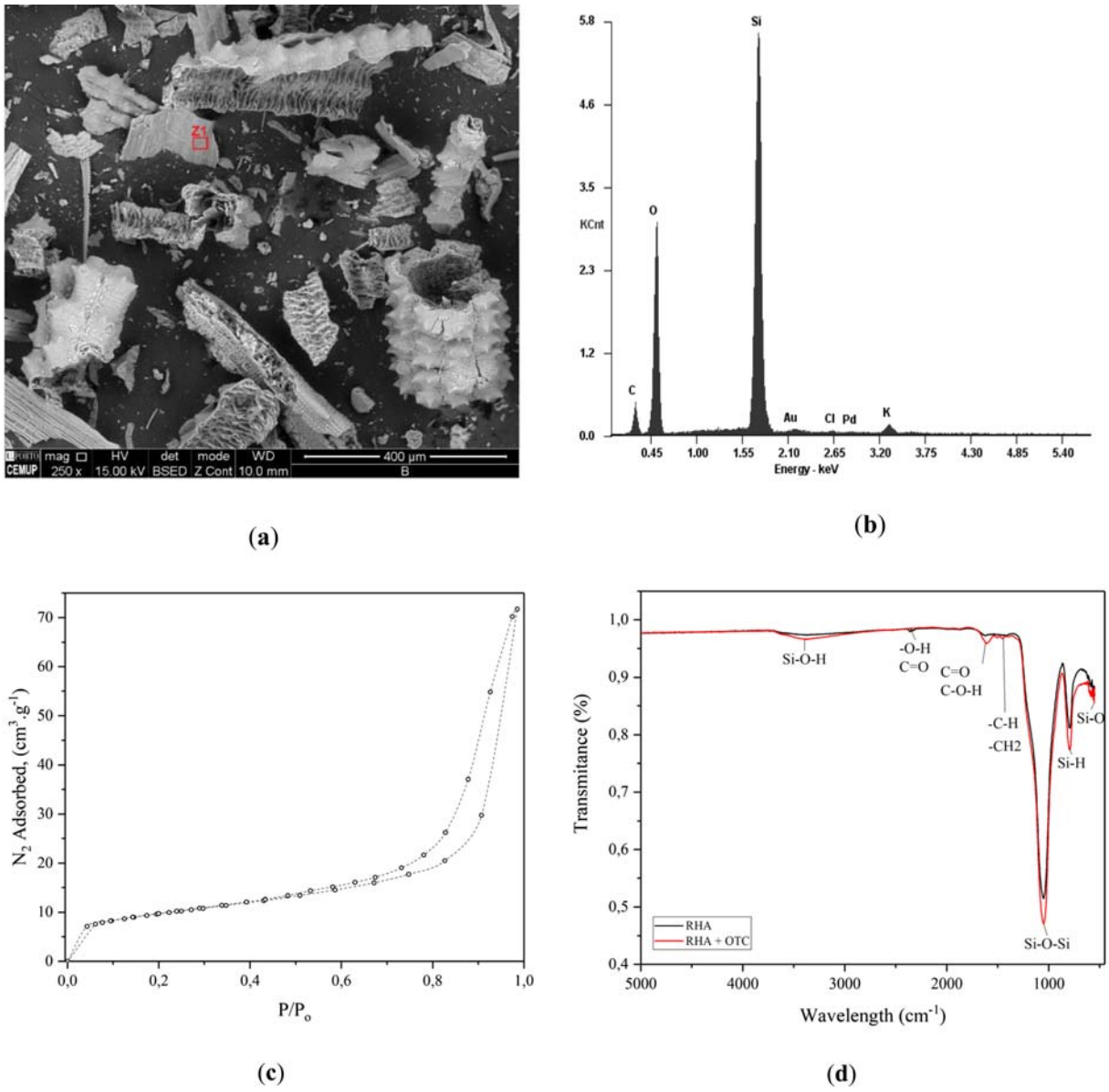

Fig. 1 Characterization of the adsorbent RHA. **a** SEM of the RHA before adsorption. **b** EDX spectrum of the RHA. **c** Nitrogen adsorption and desorption isotherm at 77 K. **d** FTIR spectroscopy of RHA before and after the OTC adsorption process

stretch of -OH or the C=O group of carboxylic acid. The peak observed at 1621.86 cm^{-1} may be owing to stretching in the groups -C=O and -COH in aldehydes and ketones, related to electrostatic interactions (Srivastava et al. 2006a). The displacement and intensity increase from 1417.54 to 1455.52 cm^{-1}, indicating the participation of the $-CH_2$ and $-CH_3$ groups. The presence of polar groups on the surface of the RHA confers the capacity of ionic adsorption and electrostatic interactions, and its stretching after adsorption indicates its participation in the process.

3.2 Adsorbent Dose Effect

There is a direct relationship between the adsorbent dose and the removal of OTC, that is, when increasing the adsorbent dose, the percentage of removal increases (Fig. 2a). This can be attributed to the increase in the

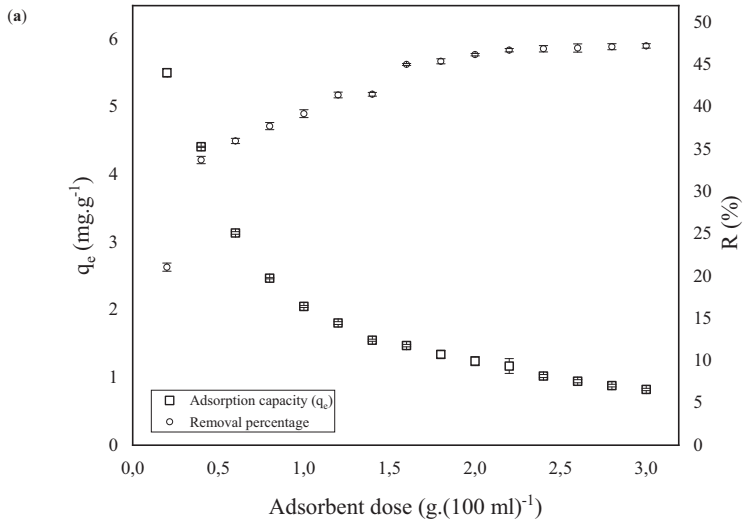

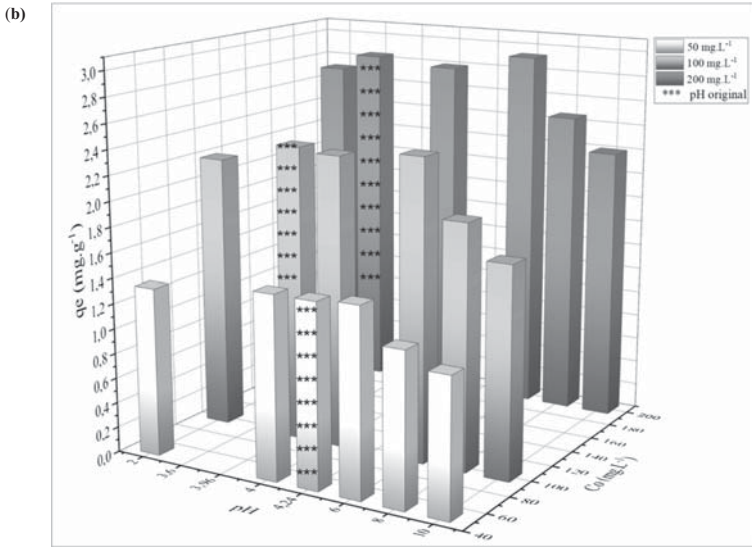

Fig. 2 **a** Adsorbent dose effect on OTC adsorption onto RHA (C_o = 50 mg L^{-1}, w = 1.6 g, t = 360 min, V = 100 mL, T = 298 K). **b** Effect of pH on OTC removal by RHA. (C_o = 50, 100, 200 mg L^{-1}, w = 1.6 g, t = 360 min, V = 100 mL, T = 298 K)

number of adsorption sites owing to the increase in mass and, therefore, in the surface area of the RHA (Aljeboree et al. 2017). From 1.6 g, the percentage of removal undergoes little variation, being virtually constant, and 1.6 g was, therefore, chosen as the optimal dose for the study of the OTC adsorption on RHA.

3.3 pH Solution Effect

The pH is a determining factor in the ionization state of the OTC, since it has several ionizable functional groups that give rise to three values of pKa (pK_{a1} = 3.57, pK_{a2} = 7.49, pK_{a3} = 9.44) (Jones et al. 2005), and its study, therefore, allows us to elucidate the mechanism of adsorption of the OTC on the RHA.

The highest adsorption capacity was observed for acidic pH, with the highest efficiency being attained at pH 6 and 4 (pKa_2) and with a slight decrease at pH 2. However, an increase in pH of up to 8 and 10 (pKa_3) causes a significant decrease in the adsorption capacity (Fig. 2b). The adsorption of OTC on RHA is, therefore, favored at a neutral and an acid pH and is negatively affected by a basic pH.

When the OTC is at a pH lower than its pKa_1 (pH < 3.5), there is a predominance of positive charges ($OTCH^+$). In the case of a solution pH < pH_{pzc}, the

surface of the adsorbent is positively charged. Since the pH_{pzc} of the RHA is 8, and for OTC solution pH < 3.5, both OTC and the RHA are positively charged. Potential electrostatic attractions are depleted between the surface of the OTC and the RHA, giving rise to a possible cation exchange mechanism. For pH 4 and 6, values between pKa_1 and pKa_2, OTC is in the form of zwitterion, which means the charge is predominantly neutral because it has both a positive and a negative charge (OTC^{+-}). At these values, the $pH < pH_{pzc}$ of the RHA (predominance of positive charges in the adsorbent) may lead to the existence of electrostatic attractions, this being the possible majority mechanism. For pH values (8 and 10) greater than pKa_2 (7.49), OTC has a predominance of negative charges (OTC^{+--} and OTC^{--}), being the $pH > pH_{pzc}$, signifying that the surface charge of the adsorbent would, therefore, be mostly negative.

The presence of negative charges in both the adsorbent and in the adsorbate favors the electrostatic repulsion, thus disfavoring the adsorption process, which explains the decrease in the adsorption capacity of RHA. In addition, the presence of hydroxyl ions generates a competition with the OTC anion for the adsorption sites, which prevents the access of the OTC (Malakootian et al. 2016).

Since the natural pH of the initial solution of OTC (3.60–4.24 for the different concentrations) is near the optimum pH, all the subsequent experiments were performed without modifying the pH values.

3.4 Contact Time Effect

The OTC concentration decreases rapidly during the first 150 min, followed by a gradual decrease, until reaching equilibrium at 420 min for lower concentrations (40–80 mg L^{-1}) and 360 min for higher concentrations (100–160 mg L^{-1}) (Fig. S2). The rapid decrease of the OTC concentration in the initial times may be attributed to the presence of a larger number of free sites on the surface of the RHA. However, when the contact time is increased, the available adsorption sites become saturated while increasing the repulsion between the OTC molecules in the liquid phase and on the surface of the RHA, and the OTC adsorption consequently decreases until it attains a constant adsorption capacity, thus confirming that the process has reached its equilibrium.

During the first minutes of the process (3–30 min), the adsorption capacity of the adsorbent behaves erratically for all the concentrations studied. Considering that OTC is very soluble in water, it is possible that in the first stages of the process a competition between the adsorbate and the solvent is established until reaching a point at which the OTC molecules manage to separate from the solvent. The adsorbate/adsorbent interactions are then favored and behave less erratically in the process. As the initial concentration rises from 20 to 160 mg L^{-1}, the adsorption capacity increases from 0.8473 to 2.7579 mg g^{-1}. This can be explained by the fact that a higher concentration of OTC in the solution facilitates a greater mass transfer driving force, thus allowing the molecules to pass easily from the aqueous phase to the surface of the adsorbent, resulting in greater adsorption.

3.5 Adsorption Kinetics

The parameters and adjustments of the kinetic models used are shown in Table 1 and Fig. 3. The PFO and PSO models did not have a good fit to the experimental data and had the lowest coefficient of determination (R^2) and the highest chi-square (x^2) values, because they underestimated the equilibrium adsorption capacity, and there was a significant difference between the values of the experimental adsorption capacity ($q_{e,exp}$) and the adsorption capacity values obtained from these theoretical models ($q_{e,cal}$) for all concentrations.

The experimental data was well fitted by the Bangham and Elovich models (Fig. 3), with a high R^2 (0.9565–0.9851) and a low x^2 (0.0357–0.4822) (Table 1). The Bangham rate constant (k_B) increases with the concentration, while the intensity of the adsorption (α) decreases, which can be observed by the fact that shorter equilibrium times were obtained for higher concentrations, owing to a higher rate of the process. The good fit observed with the Bangham model indicates that the adsorption process occurs by means of a pore diffusion mechanism. The adjustment to the Elovich model is related to the energy heterogeneity of the surface of the RHA (Yaneva et al. 2013). The increase in concentration shows an inverse relationship with the parameter β, which is related to the extension of coverage of the surface of the RHA and to the activation energy. The greater number of OTC molecules at high concentrations, therefore, cause a saturation of the adsorbent, thus reducing the number of sites available for adsorption. The Elovich parameter of α, which indicates the velocity of adsorption of the process, coincides with the trend of the Bangham rate constant, confirming that the speed of the process increases with the increase in concentration.

Table 1 Characteristic parameters, R^2 and x^2 values at different initial OTC concentrations for the Pseudo-first order, Pseudo-second order, Elovich, Bangham, and Intraparticle Diffusion kinetics models

Parameters	C_o(mg L^{-1})							
	20	40	60	80	100	120	140	160
$q_{e,exp}$	0.88	1.46	1.75	1.93	2.34	2.67	2.73	2.76
Pseudo-first order								
$q_{e,cal}$ (mg g^{-1})	0.79	1.31	1.65	1.68	2.04	2.43	2.44	2.44
k_1 (min^{-1})	0.0238	0.0168	0.0124	0.0350	0.0890	0.0536	0.0781	0.1222
R^2	0.8582	0.7653	0.7665	0.6531	0.5680	0.7780	0.7012	0.5688
x^2	0.8421	3.7166	6.6265	3.1563	1.3931	1.5366	1.3018	1.0315
Pseudo-second order								
$q_{e,cal}$ (mg g^{-1})	0.88	1.42	1.81	1.83	2.16	2.62	2.60	2.56
k_2 (g mg^{-1} min^{-1})	0.0407	0.0212	0.0116	0.0277	0.0596	0.0278	0.0413	0.0663
h (mg g^{-1} min^{-1})	0.0312	0.0428	0.0380	0.0929	0.2777	0.1901	0.2788	0.4360
R^2	0.9346	0.8632	0.8354	0.7924	0.7684	0.8850	0.8528	0.7713
x^2	0.3057	1.3080	2.7214	1.6118	0.6993	0.7501	0.6187	0.5596
Elovich								
β (g mg^{-1})	6.4255	4.0435	3.5358	3.4737	3.1817	3.1698	2.7785	2.5021
α (mg g^{-1} min^{-1})	0.0895	0.1354	0.1414	0.3937	0.7839	1.5939	2.0241	4.1837
R^2	0.9851	0.9590	0.9565	0.9574	0.9587	0.9594	0.9821	0.9673
x^2	0.0469	0.2073	0.4822	0.2942	0.1147	0.2019	0.0596	0.0780
Bangham								
k_B (mg g^{-1} $s^{-\alpha}$)	0.1719	0.2618	0.2846	0.4493	0.7620	0.8073	0.9004	1.0647
α	0.2961	0.2780	0.2698	0.2379	0.2118	0.1857	0.1742	0.1578
R^2	0.9751	0.9891	0.9708	0.9752	0.9747	0.9571	0.9825	0.9802
x^2	0.0577	0.0357	0.1486	0.1091	0.0652	0.2448	0.0503	0.0475
Intraparticle Diffusion								
K_{I1}(mg g^{-1} $min^{-0.5}$)	0.2303	0.2668	0.2562	0.3570	0.4085	0.7039	0.6222	0.4306
C_1	−0.1131	0.0307	0.1381	0.1573	0.4675	−0.0746	0.2443	0.7576
R_1^2	0.9426	0.9663	0.8159	0.8264	0.8871	0.8405	0.9421	0.9063
K_{I2}(mg g^{-1} $min^{-0.5}$)	0.1885	0.4850	0.5957	0.4038	0.4224	0.5715	0.6262	0.4394
C_2	0.0374	−0.6422	−0.8248	0.0658	0.4824	0.2554	0.1123	0.8380
R_2^2	0.9874	0.9874	0.9928	0.9691	0.9691	0.9923	0.9981	0.9721
K_{I3}(mg g^{-1} $min^{-0.5}$)	0.0792	0.2525	0.2807	0.2214	0.1274	0.1102	0.1078	0.0710
C_3	0.5001	0.2524	0.4306	0.9113	1.7218	2.1856	2.2439	2.4493
R_3^2	0.9767	0.9704	0.9459	0.9514	0.9086	0.4766	0.4023	0.6871
x^2	0.0330	0.0140	0.0625	0.0853	0.0463	0.1883	0.0270	0.0343

In order to better elucidate the adsorption mechanism, the IPD model was used. If the Weber-Morris graph (q_t vs $t^{0.5}$), which is divided into three stages, has a linear relationship and some of the stages cross the origin, the process will be controlled only by intraparticle diffusion (Tran et al. 2017). However, if the experimental data have multilinearity, the adsorption process will be controlled by two or more steps or a combination of them (Srivastava et al. 2006b). The graphs of this model for all the concentrations studied (Fig. 4) indicate that there is multilinearity (linearity in the three stages), and none of these stages in its projection passed through the origin. This experimental evidence indicates that intraparticle diffusion is not the only

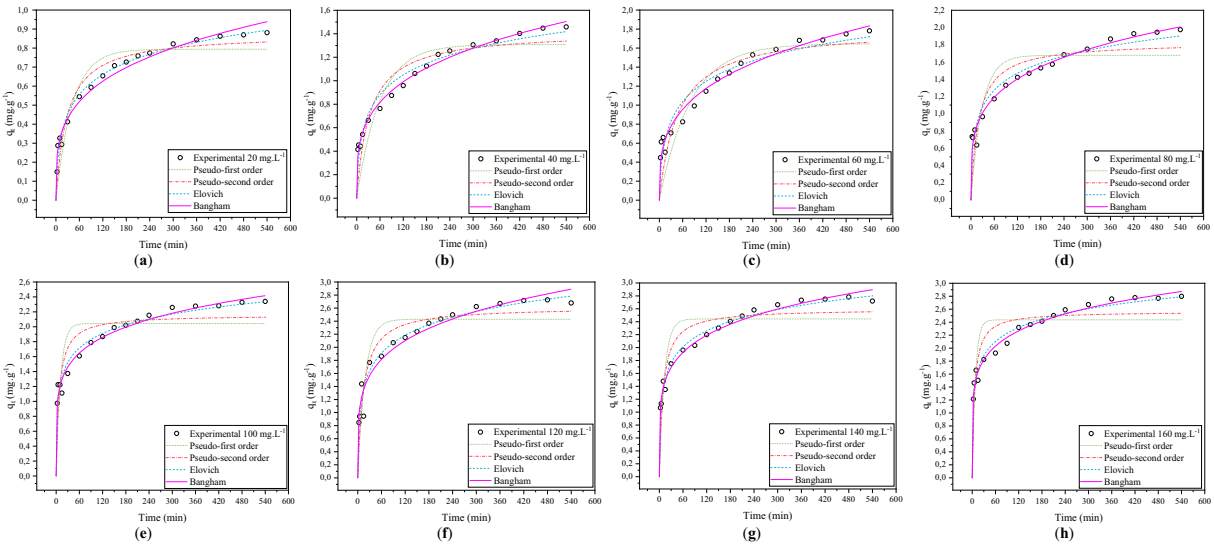

Fig. 3 PFO, PSO, Bangham, and Elovich kinetic models fitted to experimental data ($w = 1.6$ g, $V = 100$ mL, $T = 298$ K) for different initial concentrations: **a** 20 mg L^{-1}, **b** 40 mg L^{-1}, **c** 60 mg L^{-1}, **d** 80 mg L^{-1}, **e** 100 mg L^{-1}, **f** 120 mg L^{-1}, **g** 140 mg L^{-1}, **h** 160 mg L^{-1}

mechanism that controls the process, but that there are other mechanisms that occur simultaneously. The first stage of the plot shows a more pronounced inclination, attributed to mass transfer from the liquid phase to the surface of the adsorbent (film diffusion) (McKay et al. 1980). The second stage represents a gradual adsorption of the OTC onto RHA, which is associated with pore diffusion, while the last stage has a lower inclination, parallel to the x axis, which is an indicator of equilibrium, and this stage is associated with surface diffusion. The highest values of coefficient of determination (R_2^2) and diffusion constant (K_{I2}) for all concentrations were found in the second stage (Table 1), which indicates that the predominant mechanism of adsorption of OTC onto RHA is pore diffusion. This result coincides with the adequate adjustment of the Bangham model (Table 1), suggesting that the predominant mechanism is the diffusion in the pores.

3.6 Effect of Temperature

After performing the kinetic study and determining the equilibrium times as 420 and 360 min, the effect of the temperature and equilibrium of the OTC adsorption onto RHA was studied. In general, a direct relationship between the capacity of adsorption and the temperature was demonstrated for all the concentrations (Fig. S3). When the temperature increases from 298 to 328 K, the adsorption capacity increases, for all the concentrations studied. However, when increasing the temperature from 298 to 318 K, the increase in the adsorption capacity is not very significant, with values of 0.8473 to 1.0466 mg g^{-1} and 2.7579 to 3.0433 mg g^{-1} for the 20 and 160 mg L^{-1}concentrations, respectively. On the other hand, when changing the temperature from 298 to 328 K, a significant change in adsorption capacity is evidenced, with values of 0.8473 to 1.1899 mg g^{-1} and 2.7579 to 4.6662 mg g^{-1} for the same concentrations, respectively.

This experimental evidence may be owing to the fact that a greater supply of energy can break the associations between the OTC molecules and water, which causes a decrease in the viscosity of the solution resulting in an increase in the movement and velocity of diffusion of the OTC molecules in the film surrounding the RHA, at the same time as the pores expand and improve the diffusion in the pores. That is to say, the increase in energy in the process is able to reduce the restrictions in the film diffusion and the diffusion in the pores, in addition to which the OTC molecules acquire more energy with which to establish stronger interactions with the active sites of the RHA.

3.7 Adsorption Isotherms

All the equilibrium models applied had an adequate adjustment to the temperatures studied (Fig. 5a, b, c). The models that better represented the experimental data were the Sips and Redlich-Petterson (R-P) models, which had the highest R^2 and the lowest x^2 (Table 2).

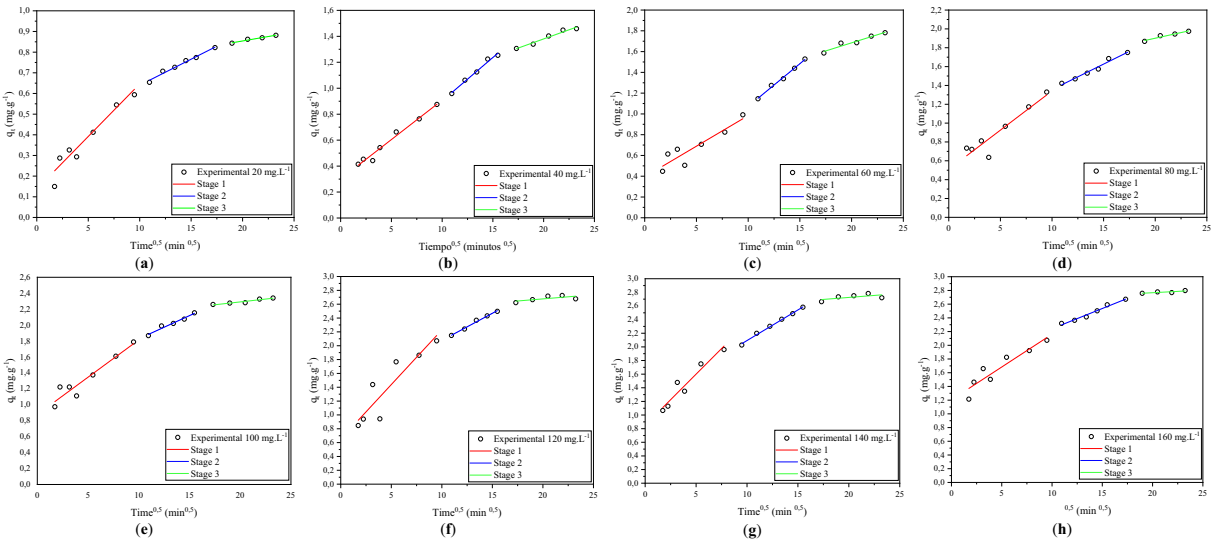

Fig. 4 IPD model. ($w = 1.6$ g, $V = 100$ mL, $T = 298$ K) for different initial concentrations: **a** 20 mg L^{-1}, **b** 40 mg L^{-1}, **c** 60 mg L^{-1}, **d** 80 mg L^{-1}, **e** 100 mg L^{-1}, **f** 120 mg L^{-1}, **g** 140 mg L^{-1}, **h** 160 mg L^{-1}

The R^2 and x^2 values of the other models applied also suggest an adequate representation of the equilibrium in the adsorption of OTC on RHA.

The adsorption equilibrium models proposed by the R-P and Sips models represent a hybrid isotherm between the Langmuir and Freundlich models. The K_{RP} adsorption constant of the R-P model increases with temperature, suggesting the presence of an endothermic process, evidenced by the increase in the adsorption capacity of the process with temperature (Fig. 5). The parameter β (R-P model) increases with the increase in temperature and approaches 1, indicating the tendency toward the Langmuir model. The equilibrium parameters (Table 2) and the adjustment to the Sips isotherm (Fig. 5) have the same trend as the R-P model, in which the constant K_S increases with the temperature, indicating that the process is favored by a greater supply of energy. The parameter $1/n$ with values < 1 verifies the heterogeneity of the adsorbent already demonstrated in the characterization.

The appropriate adjustment to the Freundlich model indicates the heterogeneity of the energy on the surface of the RHA, which is represented by the parameter n, which is also an indicator of the intensity of the adsorption. A value of $1/n$ less than 1 was reported for all the temperatures, indicating a favorable process and a high degree of heterogeneity. The highest $1/n$ (0.4141) value is found at the temperature 298 K, signifying that approximately 42% of the adsorption sites have the same energy, while the remaining 58% have different energies (Lakshmi et al. 2009). With the increase in temperature, there is a decrease in the heterogeneity of the energy of the adsorption sites, which is evidenced by the lower $1/n$ values. The K_F parameter is associated with the capacity for adsorption, and a growth of K_F with temperature is observed, which indicates that the process is favored at higher temperatures.

The separation factor calculated from the Langmuir model (R_L) decreased for all temperatures with increasing concentration, which was less than 1 and greater than zero. This result indicates that the process is favorable to the temperatures and concentrations studied. However, with the increase in concentration and temperature, the values of the separation factor are closer to zero, indicating an irreversibility of the process. The processes of physisorption are completely reversible, whereas the greater degree of irreversibility is associated with the presence of interactions of a chemical type, and this is why the increase in the temperature favors the chemisorptions mechanisms that can occur as the result of ion exchange and complexation between the OTC and RHA molecules.

3.8 Adsorption Thermodynamics

The thermodynamic parameters obtained from the equilibrium constant derived from the Langmuir and Sips models are shown in Table 3. These models were selected because they had an appropriate adjustment, a better correlation when obtaining the Kc constant and

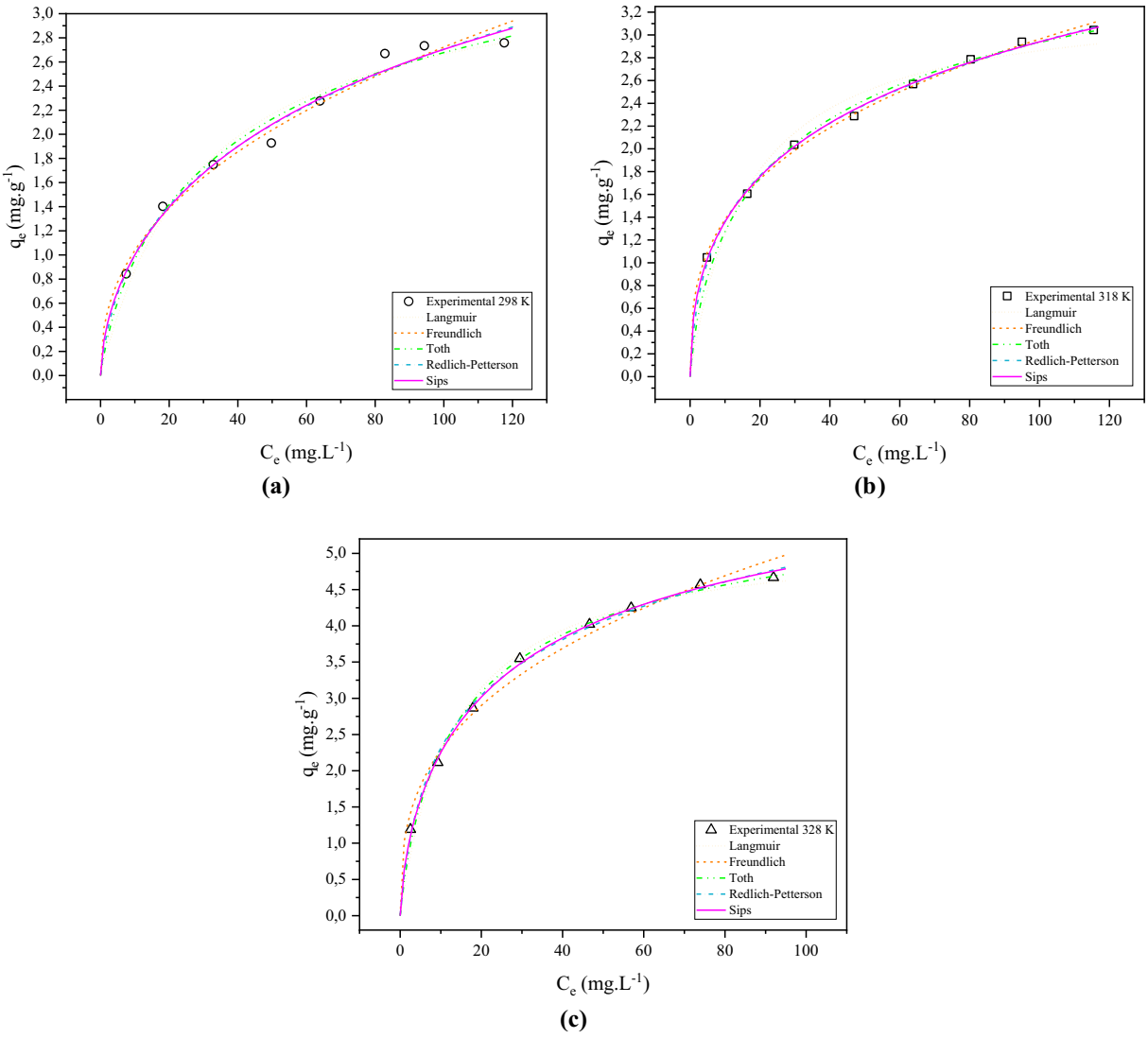

Fig. 5 Langmuir, Freundlich, Toth, Redlich-Petterson, and Sips adsorption isotherms: **a** 298 K, **b** 318 K, **c** 328 K. ($w = 1.6$ g, $V = 100$ mL, $t = 360$ min)

owing to their application in the Van't Hoff eq. (S1.Eq. 15). The thermodynamic parameters obtained by the Langmuir and Sips constant are similar as regards both sign and magnitude and have a linear regression coefficient close to 1. The $\Delta H°$ was 20.55 kJ mol^{-1}, which indicates an endothermic physical process ($\Delta H° < 40$ kJ mol^{-1}) (Tran et al. 2016). A greater supply of energy can break the adsorbate-solvent bonds, thus decreasing the viscosity of the film surrounding the adsorbent and promoting the diffusion of the adsorbate to the adsorbent. As mentioned above, the temperature can dilate the pores of the RHA, allowing large molecules of OTC to enter in them. The positive values of $\Delta S°$ reflect the increase in the randomness in the solid liquid interface in the adsorption process with the increase in the temperature. This gives the species a greater degree of freedom and makes the process more stable, thus making it more irreversible. Negative values of $\Delta G°$ were obtained, and these decrease with the increase in temperature, which indicates a feasible and spontaneous process that improves with the supply of energy.

Table 2 Adsorption isotherm parameters and R^2 and x^2 values for the Langmuir, Freundlich, Toth, Redlich-Petterson, and Sips isotherms at 298, 318, and 328 K

Isotherms	Parameters	Temperature (K)		
		298	318	328
Langmuir	Q_{max}(mg g^{-1})	3.3426	3.4561	5.2863
	K_L(L mg^{-1})	0.0336	0.0595	0.0733
	R_L	0.58–0.16	0.44–0.09	0.38–0.07
	R^2	0.9634	0.9513	0.9841
	x^2	0.0792	0.1504	0.1690
Freundlich	K_F [(mg g^{-1}).(L $mg^{-1})^{1/n}$]	0.4043	0.6409	1.0266
	$1/n$	0.4141	0.3325	0.3467
	R^2	0.9772	0.9968	0.9807
	x^2	0.0371	0.0050	0.0790
Toth	Q_{max}	4.7956	5.0690	6.2643
	K_T	0.0470	0.1000	0.1002
	n	0.5838	0.5013	0.6830
	R^2	0.9769	0.9856	0.9942
	x^2	0.0364	0.0478	0.0512
Redlich-Petterson (R-P)	K_{RP} (L g^{-1})	0.3165	0.7194	0.7479
	α (L $mg^{-1})^{\beta}$	0.4360	0.7836	0.3486
	β	0.6950	0.7382	0.8074
	R^2	0.9805	0.9968	0.9954
	x^2	0.0286	0.0064	0.0219
Sips	Q_{max} (mg g^{-1})	6.6153	6.9424	7.2893
	K_s (L mg^{-1})	0.0457	0.0778	0.1000
	$1/n$	0.5901	0.4695	0.6809
	R^2	0.9808	0.9977	0.9975
	x^2	0.0290	0.0036	0.0126

Table 3 Thermodynamic parameters of OTC adsorption onto RHA

Temperature (K)	ΔG° (kJ mol^{-1})	ΔH° (kJ mol^{-1})	ΔS° (J mol^{-1})
Langmuir *(R^2 = 0.9959)*			
298	− 33,9368	22,5840	189,7475
318	− 37,8374		
328	− 39,5952		
Sips *(R^2 = 0.9996)*			
298	− 34,8547	20,5513	185,9043
318	− 38,5441		
328	− 40,4411		

3.9 Mechanism of Adsorption

The amphoteric nature of OTC allows the existence of different ionic species at different pH values. Since the best results were obtained at pH 4–6, the OTC adsorption mechanism on RHA associated with these pH values will be explained. In this pH range ($pKa_1 < pH < pKa_2$), OTC is in its zwitterion form, which has positive and negative charges that are neutralized to obtain a neutral final charge. Furthermore, upon considering the pH_{pzc} of RHA (8) and the natural pH of the initial solution (3.60–4.24), the adsorption process occurs at $pH < pH_{pzc}$, and in these conditions, the surface of the RHA is predominantly positively charged, which allows weak electrostatic interactions with the OTC. This mechanism may occur by means of:

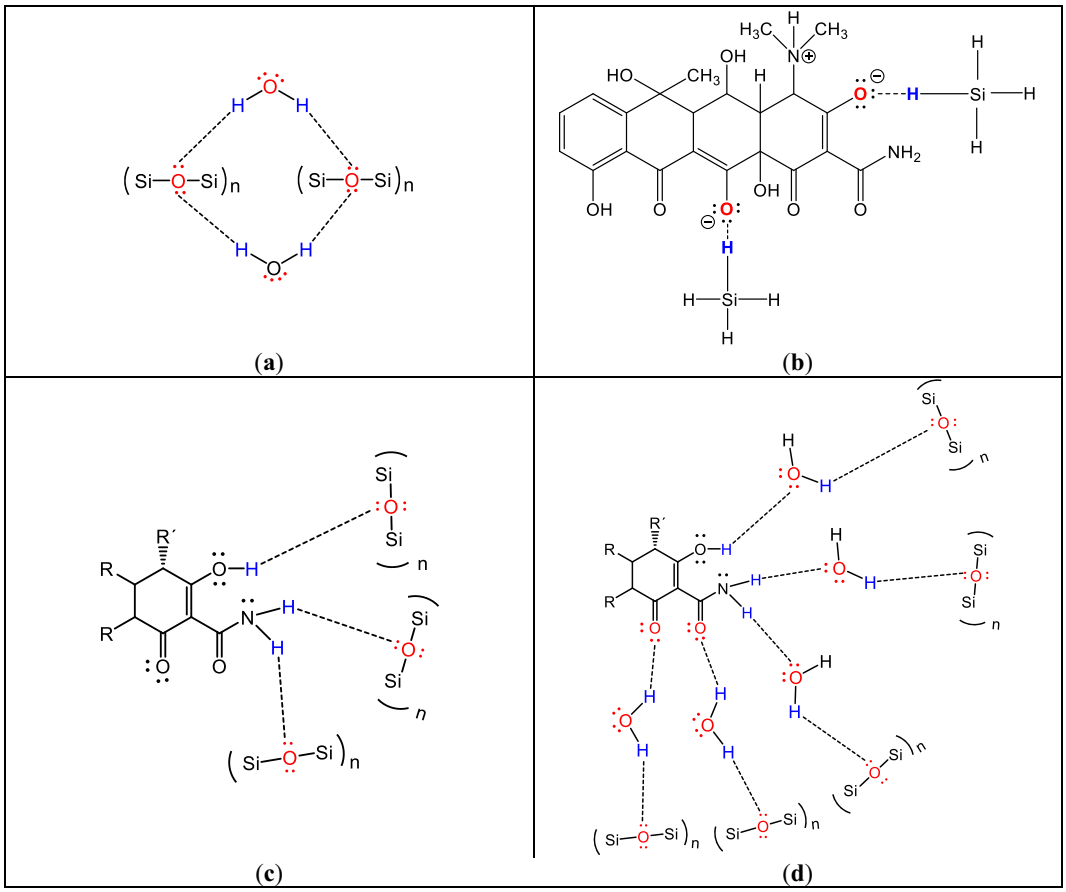

Fig. 6 Mechanism of adsorption of OTC onto RHA. **a** Interaction of water molecules with RHA surface. **b** Electrostatic interaction between OTC and RHA. **c** Formation of hydrogen bonds through direct interaction with the RHA. **d** Formation of hydrogen bonds through intermediation of water molecules

(i) Electrostatic interactions between the hydroxyl groups of the tricarbonyl system and the phenolic diketone of the OTC with the cations (H^+) of the silane groups present on the surface of the RHA (Fig. 6b).

(ii) The formation of Hydrogen bonds between the amine and hydroxyl groups of the phenolic diketone of the OTC and the oxygens in the siloxane groups on the surface of the RHA (Fig. 6c) or by the intermediation of water molecules, which bond both with the OTC molecule and the siloxane groups on the surface of the RHA (Fig. 6d). The water molecules can interact by themselves with the RHA, creating hydrogen bonds with the siloxane groups and competing with the OTC for the adsorption sites (Fig. 6a). As proven in the thermodynamic study, the heat increase can break the OTC-H_2O and H_2O-RHA bonds, thus allowing the OTC molecules to reach the surface of the RHA and enter the pores to establish stronger bonds, which favors the adsorption process. The positive $\Delta S°$ obtained indicates a more irreversible process with the increase in heat, which can be associated with the presence of chemical-like interactions, and the increase in temperature, therefore, favors a chemisorption mechanism by means of an ion exchange and complexation between the OTC and the RHA molecules.

(iii) An acid-basic reaction mechanism between RHA silicates, which act as Lewis bases, and the hydroxyl groups in the OTC tricarbonyl system, forming conjugated pairs that can follow the path indicated in (i) (Fig. 7).

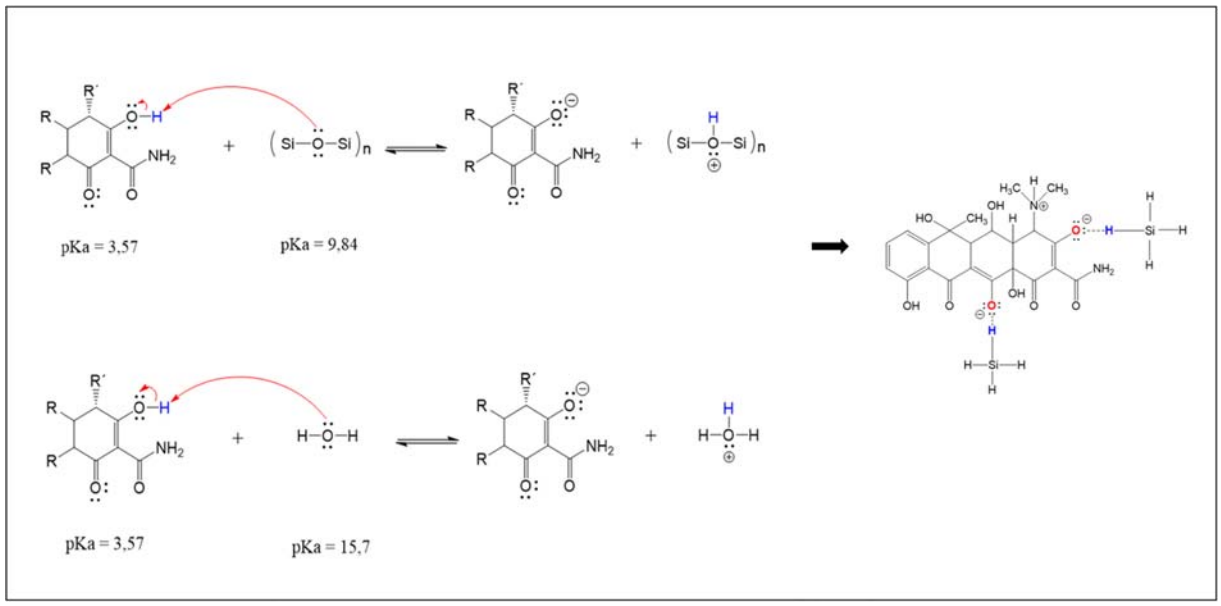

Fig. 7 Lewis acid-base reaction between. **a** OTC and siloxane group. **b** OTC and water

4 Conclusions

The RHA used in this study has a heterogeneous fibrous and porous structure composed mainly of silica. The good fit of the experimental data to the Bangham and Elovich models and the multilinearity shown by the Weber-Morris chart (IPD model) indicate that the OTC adsorption onto RHA occurs by means of diffusion in the film in the first stage and the diffusion in the pores in the second stage, ending with a very rapid adsorption stage. The equilibrium of the process was well represented by the R-P and Sips model, which indicates the energetic heterogeneity of the surface of the RHA and the endothermic nature of the process. The isotherms parameters at different temperatures showed that, although the process occurred by means of physisorption at room temperature, the increase in temperature may allow the occurrence of processes of chemisorption. The removal of OTC was highly influenced by the pH solution, which was favored at acidic pH values. The adsorption of OTC is a feasible spontaneous and endothermic process, in which the mechanism could take place thanks to ion exchange and electrostatic attractions.

Acknowledgments The authors would like to thank the Laboratório de Engenharia e Processos Ambientais (LEPA), Laboratório de Engenharia Ambiental (LEA), Centro de Tecnologías Estratégicas do Nordeste (CETENE), and Laboratory of the Centro de Materiais da Universidade do Porto (CEMUP) for their help in the adsorbent characterization and the Scanning Electron Microscopy and X-ray microanalyses and to the company Espectrocrom, especially to the Engineer Edmundo Regalado by his unconditional support.

Funding Information The authors would like to acknowledge the Secretaría de Nacional de Educación Superior, Ciencia y Tecnología del Ecuador (SENESCYT), and Universidad Técnica de Manabí for the financial support granted for this work.

References

Acevedo, B., Barriocanal, C., Lupul, I., & Gryglewicz, G. (2015). Properties and performance of mesoporous activated carbons from scrap tyres, bituminous wastes and coal. *Fuel, 151*, 83–90. https://doi.org/10.1016/j.fuel.2015.01.010.

Ahmaruzzaman, M., & Gupta, V. K. (2011). Rice husk and its ash as low-cost adsorbents in water and wastewater treatment. *Industrial & Engineering Chemistry Research, 50*(24), 13589–13613. https://doi.org/10.1021/ie201477c.

Ahmed, M. J. (2017). Adsorption of quinolone, tetracycline, and penicillin antibiotics from aqueous solution using activated carbons: Review. *Environmental Toxicology and Pharmacology, 50*, 1–10. https://doi.org/10.1016/j.etap.2017.01.004.

Ahmed, M. B., Zhou, J. L., Ngo, H. H., & Guo, W. (2015). Adsorptive removal of antibiotics from water and wastewater: Progress and challenges. *Science of The Total Environment, 532*(supplement C), 112–126. https://doi.org/10.1016/j.scitotenv.2015.05.130.

Aljeboree, A. M., Alshirifi, A. N., & Alkaim, A. F. (2017). Kinetics and equilibrium study for the adsorption of textile dyes on coconut shell activated carbon. *Arabian Journal of*

Chemistry, 10, S3381–S3393. https://doi.org/10.1016/j.arabjc.2014.01.020.

Álvarez-Torrellas, S., Rodríguez, A., Ovejero, G., & García, J. (2016). Comparative adsorption performance of ibuprofen and tetracycline from aqueous solution by carbonaceous materials. *Chemical Engineering Journal, 283*(supplement C), 936–947. https://doi.org/10.1016/j.cej.2015.08.023.

Bhowmick, A. C., Rahaman, M. A., Islam, M., Akther, N., Hossain, M. S., & Patwary, M. M. (2015). Comparative adsorption study on rice husk and rice husk ash by using amaranthus gangeticus pigments as dye. *European Scientific Journal, ESJ, 11*(21).

Brunauer, S., Deming, L. S., Deming, W. E., & Teller, E. (1940). On a theory of the van der Waals adsorption of gases. *Journal of the American Chemical Society, 62*(7), 1723–1732. https://doi.org/10.1021/ja01864a025.

Cheng, D.-H., Yang, S.-K., Zhao, Y., & Chen, J. (2013). Adsorption behaviors of Oxytetracycline onto sediment in the Weihe River, Shaanxi, China. *Journal of Chemistry, 2013*.

Cristiano, E., Hu, Y.-J., Siegfried, M., Kaplan, D., & Nitsche, H. (2011). A comparison of point of zero charge measurement methodology. *Clays and Clay Minerals, 59*(2), 107–115. https://doi.org/10.1346/CCMN.2011.0590201.

Foo, K. Y., & Hameed, B. H. (2009). Utilization of rice husk ash as novel adsorbent: A judicious recycling of the colloidal agricultural waste. *Advances in Colloid and Interface Science, 152*(1–2), 39–47. https://doi.org/10.1016/j.cis.2009.09.005.

Hadipramana, J., Riza, F. V., Rahman, I. A., Loon, L. Y., Adnan, S. H., & Zaidi, A. M. A. (2016). Pozzolanic characterization of waste Rice husk ash (RHA) from Muar, Malaysia. *IOP Conference Series: Materials Science and Engineering, 160*(1), 012066.

Halling-Sørensen, B., Sengeløv, G., & Tjørnelund, J. (2002). Toxicity of tetracyclines and tetracycline degradation products to environmentally relevant bacteria, including selected tetracycline-resistant bacteria. [journal article]. *Archives of Environmental Contamination and Toxicology, 42*(3), 263–271. https://doi.org/10.1007/s00244-001-0017-2.

Jaerger, S., dos Santos, A., Fernandes, A. N., & Almeida, C. A. P. (2015). Removal of p-Nitrophenol from aqueous solution using Brazilian peat: Kinetic and thermodynamic studies. *Water, Air, & Soil Pollution, 226*(8), 236. https://doi.org/10.1007/s11270-015-2500-9.

Jones, A. D., Bruland, G. L., Agrawal, S. G., & Vasudevan, D. (2005). Factors influencing the sorption of oxytetracycline to soils. *Environmental Toxicology and Chemistry, 24*(4), 761–770. https://doi.org/10.1897/04-037R.1.

Kong, W., Li, C., Dolhi, J. M., Li, S., He, J., & Qiao, M. (2012). Characteristics of oxytetracycline sorption and potential bioavailability in soils with various physical-chemical properties. *Chemosphere, 87*(5), 542–548. https://doi.org/10.1016/j.chemosphere.2011.12.062.

Lakshmi, U. R., Srivastava, V. C., Mall, I. D., & Lataye, D. H. (2009). Rice husk ash as an effective adsorbent: Evaluation of adsorptive characteristics for indigo carmine dye. *Journal of Environmental Management, 90*(2), 710–720. https://doi.org/10.1016/j.jenvman.2008.01.002.

Leal, J. F. (2017). *Fotodegradação de contaminantes como meio de remediação de águas de aquacultura*. Aveiro: Universidade de Aveiro.

Li, R., Jia, Y., Wu, J., & Zhen, Q. (2015). Photocatalytic degradation and pathway of oxytetracycline in aqueous solution by Fe 2 O 3–TiO 2 nanopowder. *RSC Advances, 5*(51), 40764–40771.

Malakootian, M., Bahraini, S., & Zarrabi, M. (2016). Removal of tetracycline antibiotic from aqueous solutions using modified pumice with magnesium chloride. *Jentashapir Journal Of Health Research*, e37583.

McKay, G., Otterburn, M. S., & Sweeney, A. G. (1980). The removal of colour from effluent using various adsorbents—III. Silica: Rate processes. *Water Research, 14*(1), 15–20. https://doi.org/10.1016/0043-1354(80)90037-8.

Mihciokur, H., & Oguz, M. (2016). Removal of oxytetracycline and determining its biosorption properties on aerobic granular sludge. *Environmental Toxicology and Pharmacology, 46*(supplement C), 174–182. https://doi.org/10.1016/j.etap.2016.07.017.

Monteros, A., Sumba, E., & Salvador, S. (2014). *Productividad agrícola en el Ecuador*. Quito: MAGAP.

Park, B.-D., Wi, S. G., Lee, K. H., Singh, A. P., Yoon, T.-H., & Kim, Y. S. (2003). Characterization of anatomical features and silica distribution in rice husk using microscopic and micro-analytical techniques. *Biomass and Bioenergy, 25*(3), 319–327. https://doi.org/10.1016/S0961-9534(03)00014-X.

Ratasuk, N., Boonsaner, M., & Hawker, D. W. (2012). Effect of temperature, pH and illumination on abiotic degradation of oxytetracycline in sterilized swine manure. *Journal of Environmental Science and Health, Part A, 47*(11), 1687–1694.

Rodríguez-Díaz, J. M., García, J. O. P., Sánchez, L. R. B., da Silva, M. G. C., da Silva, V. L., Arteaga-Pérez, L. E. (2015). Comprehensive characterization of sugarcane bagasse ash for its use as an adsorbent. *BioEnergy Research, 8*(4), 1885–1895.

Santaeufemia, S., Torres, E., Mera, R., & Abalde, J. (2016). Bioremediation of oxytetracycline in seawater by living and dead biomass of the microalga Phaeodactylum tricornutum. *Journal of Hazardous Materials, 320*, 315–325. https://doi.org/10.1016/j.jhazmat.2016.08.042.

Song, Y., Sackey, E. A., Wang, H., & Wang, H. (2019). Adsorption of oxytetracycline on kaolinite. *PLoS One, 14*(11), e0225335. https://doi.org/10.1371/journal.pone.0225335.

Srivastava, V. C., Mall, I. D., & Mishra, I. M. (2006a). Characterization of mesoporous rice husk ash (RHA) and adsorption kinetics of metal ions from aqueous solution onto RHA. *Journal of Hazardous Materials, 134*(1), 257–267. https://doi.org/10.1016/j.jhazmat.2005.11.052.

Srivastava, V. C., Swamy, M. M., Mall, I. D., Prasad, B., & Mishra, I. M. (2006b). Adsorptive removal of phenol by bagasse fly ash and activated carbon: Equilibrium, kinetics and thermodynamics. *Colloids and Surfaces A: Physicochemical and Engineering Aspects, 272*(1–2), 89–104.

Tran, H. N., You, S.-J., & Chao, H.-P. (2016). Thermodynamic parameters of cadmium adsorption onto orange peel calculated from various methods: A comparison study. *Journal of Environmental Chemical Engineering, 4*(3), 2671–2682. https://doi.org/10.1016/j.jece.2016.05.009.

Tran, H. N., You, S.-J., Hosseini-Bandegharaei, A., & Chao, H.-P. (2017). Mistakes and inconsistencies regarding adsorption of contaminants from aqueous solutions: A critical review.

Water Research, 120, 88–116. https://doi.org/10.1016/j.watres.2017.04.014.

Villar da Gama, B. M., Elisandra do Nascimento, G., Silva Sales, D. C., Rodríguez-Díaz, J. M., Bezerra de Menezes Barbosa, C. M., & Menezes Bezerra Duarte, M. M. (2018). Mono and binary component adsorption of phenol and cadmium using adsorbent derived from peanut shells. *Journal of Cleaner Production, 201*, 219–228. https://doi.org/10.1016/j.jclepro.2018.07.291.

Wang, D., Xu, H., Yang, S., Wang, W., & Wang, Y. (2018). Adsorption property and mechanism of Oxytetracycline onto willow residues. *International Journal of Environmental Research and Public Health, 15*(1), 8.

Yaneva, Z., Koumanova, B., & Allen, S. (2013). Applicability comparison of different kinetic/diffusion models for 4-nitrophenol sorption on Rhizopus oryzae dead biomass. *Bulgarian Chemical Communications, 45*(2), 161–168.

Zhang, X., Guo, W., Ngo, H. H., Wen, H., Li, N., & Wu, W. (2016). Performance evaluation of powdered activated carbon for removing 28 types of antibiotics from water. *Journal of Environmental Management, 172*(supplement C), 193–200. https://doi.org/10.1016/j.jenvman.2016.02.038.